The reduction of copper in porous matrices - The role of electrostatic stabilisation

O. P. Tkachenko[a], K. V. Klementiev[b], M. W. E. van den Berg, H. Gies[c], W. Grünert

Lehrstuhl für Technische Chemie, Ruhr-Universität Bochum, Bochum, Germany (w.gruenert@techem.rub.de), [a]on leave from: N. D. Zelinsky Institute of Organic Chemistry, Russian Academy of Sciences, Moscow, Russia, [b]Hasylab, Hamburg, Germany, [c]Lehrstuhl für Kristallographie, Ruhr-Universität Bochum,

*Corresponding Author:

Prof. W. Grünert, Lehrstuhl für Technische Chemie, Ruhr-Universität Bochum, P. O. Box 102148, D-44780 Bochum, Germany, Tel. +49 234 322 2088, Fax +49 234 321 4115, email w.gruenert@techem.ruhr-uni-bochum.de

Running title: Reduction of Cu(II) in faujasite matrices

Keywords: Cu-Y; Cu in siliceous Y; Cu reduction; electrostatic stabilisation; Cu reduction, influence of zinc on; TPR; XAFS

Abstract

The redox properties of Cu(II) species in FAU matrices have been studied by temperature programmed reduction (TPR) in hydrogen and by XAFS analysis of the products obtained after (stationary) reduction treatments at various temperatures. The influence of the matrix polarity was investigated by comparing alumosilicate FAU (Y zeolite) with siliceous FAU. In addition, the influence of Zn ions on the reduction process was studied. It was found that both the matrix composition and the presence of zinc ions exert a significant influence on the course of the reduction. In Y zeolite, heat treatment which is known to transfer Cu(II) ions to remote sites (S_I, $S_{I'}$, $S_{II'}$) affects the reduction process dramatically. Cu(II) is most easily reduced in siliceous FAU, but the reduction proceeds in two clearly separated steps. Between these steps, small Cu(0) nuclei coexist with Cu(I) species, apparently unable to activate hydrogen for the autocatalytic reduction of the remaining Cu ions. The polarity of the matrix causes an upshift of the Cu(II) reduction temperature (in TPR by ≈80 K for sites in the large cavity, by ≈105 K for the remote sites), but the reduction of Cu(I) depends strongly on the simultaneous presence of Cu(0) and on its ability to activate hydrogen and induce an autocatalytic reduction mechanism. While Cu(I) species in the large cavities are easily reduced to the metal, tending to segregate from the zeolite lattice, Cu(I) ions in remote sites are strongly stabilized towards further reduction and even traces of Cu metal form only at very high temperatures. In the presence of zinc ions, the Cu metal particles formed were found to be smaller than in zinc-free samples.

Introduction

The extensive attention for copper-modified zeolites as catalysts for environmental and other reactions of technical interest has induced a variety of investigations into the reduction behaviour of Cu(II) species in microporous alumosilicate matrices[1-8]. Temperature-programmed reduction (TPR) was the most frequently used tool in these studies[1-4], but investigations by XAFS and photoemission techniques are known as well[4,5,7,8]. As opposed to bulk CuO, Cu(II) in microporous alumosilicate matrices is reduced in two steps, which have been attributed to the reduction steps Cu(II) $\rightarrow$ Cu(I) and Cu(I) $\rightarrow$ Cu(0). The stabilisation of cations in the intrinsic electrostatic field of the zeolite matrix provides a convenient explanation for this observation. For the Y zeolite, it is known that the second reduction step proceeds only at very high temperatures[6], which may be attributed to a particular stabilisation exerted on the cations at the remote sites in the hexagonal prisms (S_I) or in the sodalite cages ($S_{I'}$, $S_{II'}$).

We have previously demonstrated that the two-step reduction scheme is not particular for alumosilicate zeolites but occurs in siliceous MFI (silicalite-1) as well[9]. Moreover, during the reduction of Cu(II) oxide clusters deposited into silicalite-1, Cu(0) nuclei were present already after the first reduction step without triggering an accelerated (autocatalytic) reduction of the remaining Cu(I) ions upon a temperature increase of almost 100 K. Together with related observations in the course of Cu(II) reduction in ZSM-5 and in MCM-48 (of different Cu content) this result gave rise to the conclusion that Cu metal nuclei are unable to activate hydrogen below a critical particle size.

During the work with the MFI matrices, a significant stabilisation of Cu ions that might be attributed to the intra-zeolite electrostatic potential was not observed. A more pronounced influence can be expected in zeolites with higher Al content, e.g. Y. With the FAU structure, the influence of the remote cation sites on the course of the reduction is an additional interesting feature. We report here studies on the reduction of Cu(II) in dealuminated as well as in alumosili-

cate FAU. The influence of the remote sites has been traced by starting from Cu-Y samples in calcined or in uncalcined initial state. Additionally, the influence of Zn ions on the reduction of Cu(II) ions has been investigated for siliceous and alumosilicate FAU. Cu- and Zn-exchanged zeolites have been described as catalysts for the water gas shift reaction[10]. The present context is an effort to create model methanol synthesis catalysts by incorporating the Cu/ZnO system into micro- or mesoporous matrices. More results of this project are published elsewhere[11-14].

Experimental

Materials. Dealuminated Y ("DA-Y") was a material produced by Degussa AG via the $SiCl_4$ dealumination route, which avoids the creation of mesopores. The Si/Al ratio is 120. Na-Y (Si/Al = 2.3) was kindly donated by Chemiewerk Bad Köstritz (Germany).

Cu-Y was prepared under different conditions to obtain Cu ions predominantly in the large cavity or at remote sites. The first case was targeted by exchanging Na-Y once with a 0.01 M aqueous Cu acetate solution at room temperature for 24 h and drying the washed product at 333 K for 6 days ("CuNa-Y(D)"). A somewhat higher Cu loading was intended for the calcined Cu-Y sample ("CuNa-Y(C))") by exchanging Na-Y twice with the same copper acetate solution at 373 K for 7h. After each exchange step, the washed zeolite was dried overnight and subjected to a thermal treatment in nitrogen to induce migration of Cu ions to the remote sites (0.5 K/min to 673 K, with a 4 h isothermal period). Finally, CuNa-Y(C) was calcined in synthetic air (20 % O_2 in N_2) at 673 K.

The introduction of Cu into DA-Y was achieved with a procedure similar to that used for the silicalite matrix previously[9], which is based on the mobility of Cu(I) species at high temperatures[15]. DA-Y was three times soaked in a 0.01 M ethanolic copper acetate solution at 333 K for 22 h. After each impregnation, the material was dried and heated in flowing N_2 at 823 K for 4 h to induce the reduction of Cu(II) to Cu(I) and the diffusion of the latter into the pore system. Finally, the sample was calcined in synthetic air at 673 K.

Zinc was introduced into DA-Y by reacting it (after drying at 453 K in vacuum for 17 h) with a 2 M solution of $Zn(C_2H_5)_2$ in pentane, followed by calcination in synthetic air at 823 K[12]. Copper was additionally deposited into this sample by a procedure analogous to that used for the pure DA-Y (*vide supra*), however with impregnation in aqueous Cu acetate solution at 373 K and all thermal treatments performed at 823 K. The ZnCu-Y sample was prepared in a two-step sequence as well, with Zn introduced first by threefold ion exchange with a 1.6 M aqueous zinc acetate solution at 373 K for 7 h, followed by drying and thermal treatment in nitrogen at 673 K (4 h, temperature ramp 0.5 K/min). The copper was then added by analogous threefold ion exchange with the 0.01 M aqueous Cu acetate solution under reflux, with analogous intermediate thermal treatments in N_2 at 673 K and final calcination in synthetic air at 673 K.

The Cu and Zn contents of the samples as obtained by ICP-OES and confirmed by assessments via the step heights (Cu*K* and Zn*K*) in the XAFS spectra are summarized in Table 1.

Methods. The distribution of Cu and Zn species in the initial materials was investigated by a combination of XPS and X-ray-induced Auger electron spectroscopy (XAES). The spectra were measured with a Leybold LH 10 spectrometer equipped with an EA 10/100 multi-channel detector (Specs), using MgKα irradiation (10 kV, 20 mA). Spectra were referenced to the Si(2p) line as an internal reference, which was set to 103.3 eV for the siliceous DA-Y and to 102.6 eV for the Y zeolite[16]. In the combination of XPS and XAES, an intra-zeolite location of Cu ions can be identified by an Auger parameter α_{Cu} (sum of Cu LVV kinetic Auger energy and Cu 2p XPS binding energy) significantly below those of the bulk Cu oxides[7,17,18]. Unfortunately, this method is not applicable to the zinc component, which has to be, therefore, assessed on the basis of elemental ratios in the XPS sampling region alone. These ratios were derived from line intensity ratios using Scofield interaction cross sections[19] together with an empirical function describing the energy dependence of the analyser transmittance of the instrument used.

TPR was performed with a mixture containing 4.2 vol-% H_2 in He (84 ml/min), ramping the temperature at 10 K/min from room temperature to 1070 K. The H_2 content of the effluent was measured by a catharometry-based instrument (Hydros, Fisher-Rosemount). For technical reasons, the TPR profiles of the Zn-containing samples had to be measured in a slightly different setup that permitted maximum temperatures of 773 K only. The compatibility of the results in the two setups has been demonstrated in a previous paper [9].

Cu*K* and Zn *K* XAFS spectra (edges at 8.979 and 9.659 keV) were measured in transmission mode at Hasylab E4 station (Hamburg) using a Si(111) double crystal monochromator (detuned to give 50 % of maximum intensity for higher harmonics suppression). The experiments were performed with an *in-situ* cell described earlier[20]. In a typical experiment, a sample was heated in flowing diluted hydrogen (5 % in He) to the first reduction temperature at 5 K/min and kept there for 15 minutes (stationary reduction regime). After cooling to liquid nitrogen temperature, the spectrum of the absorption coefficient μ was taken twice (recording simultaneously the spectrum of a Cu (Zn) foil between the second and a third ionisation chamber for energy calibration). Subsequently, the sample was heated to the previous reduction temperature at 10 K/min, and the next temperature was established with 5 K/min.

Data treatment was carried out using the software package VIPER[21]. A Victoreen polynomial was fitted to the pre-edge region for background subtraction. The smooth atomic background μ_0 was estimated using a smoothing cubic spline. The Fourier analysis of the k^2-weighted experimental function $\chi = (\mu-\mu_0)/\mu_0$ was performed with a Kaiser window. For the determination of structural parameters, theoretical references calculated by the FEFF8.10 code[22] were used. To minimize the number of free parameters, equal backscatters were fitted with the same E_o-shift wherever possible. The influence of the Cu EXAFS on the nearby Zn spectrum was tested with a representative sample with similar Cu and Zn contents, the Cu having been reduced to the metal state (the particular sample was supported on mesoporous MCM-48[14]). For this test, the model parameters for the Cu nanoparticles were extracted from the Cu*K* spectrum, which was then simulated in full length (i.e. extending over the Zn*K* edge) with these data and

subtracted from the Zn*K* XAFS. The comparison between uncorrected and corrected Zn EXAFS showed that the influence of the copper on the zinc spectrum is negligible under these conditions, which are similar to those encountered in the present study.

Results

XPS / XAES of initial samples. The surface-analytical investigation of the initial samples is summarized in Fig. 1 and Table 1. The figure shows the kinetic energy region where CuLVV Auger lines are expected, but also the Na KL_1L_1 and various Zn Auger lines. In all spectra, the Cu Auger line appears at a much lower kinetic energy (K.E.) than expected for CuO or Cu_2O, which is reflected in very low Auger parameters (Table 1). This shift suggests an intraporous location of the Cu species[7,8,17,18], extra-zeolite oxide aggregates have not been formed to a significant extent in any of the samples including ZnCu-Y where Cu is enriched in the external surface region. With the remaining samples, the comparison between surface and bulk Cu/Si ratios confirms that copper is well distributed over the pore systems (Table 1). In CuNa-Y(C), the surface region was even significantly depleted in Cu – unlike the uncalcined sample. Unfortunately, the Zn Auger lines are not sensitive to extreme disorder or quasi-atomic dispersion of the Zn species. However, a largely homogeneous distribution of the zinc over the pore systems may be concluded from the absence of dramatic surface enrichment effects as well (Table 1).

Assuming a stoichiometry of Me/Al = 0.5, ZnCu-Y is fully exchanged with Zn/Cu ions. Its strong surface enrichment in Cu (and still notable enrichment in Zn) indicates therefore that the surface region is significantly over-exchanged. While the formation of bulk CuO aggregates is excluded by the Auger spectra (*vide supra*), the presence of bulk ZnO aggregates cannot be excluded from the surface-analytical data. The EXAFS spectrum of the initial sample (Fig. 6a) proves, however, the absence of well-ordered zinc oxide structures.

Temperature-programmed reduction. In Figure 2, the TPR profiles (H_2 consumption related to Cu content) of Cu(II) in FAU matrices are compared with that of bulk CuO, which is reduced in one very narrow peak below 470 K. In the zinc-free samples, the zeolite-supported Cu(II) spe-

cies are all reduced in two steps, but there are significant differences between the materials studied. In the siliceous DA-Y, the reduction starts at the lowest temperature. With the Y matrix, the onset is by 60-80 K higher (peak temperatures differing by 80 and 105 K, respectively). As expected, the profiles for the dried and the calcined CuNa-Y differ strongly. It should be, noted, however, that the first reduction step occurs at almost the same temperature in both cases while the second step is strongly retarded in CuNa-Y(C). In CuNa-Y(D), the two reduction steps are almost merged into one while they are well separated with Cu-DAY and CuNa-Y(C). The presence of zinc changes the reduction kinetics strongly. In the DA-Y matrix, the reduction of copper starts at higher temperature than in absence of Zn. Only one reduction peak is observed, the second one has been transformed into a pronounced tailing. In ZnCu-Y, the first reduction signal is much steeper, and a second peak emerges weakly on the tailing.

X-ray absorption. Figures 3 and 4 present examples of Cu*K* XAFS spectra measured after the reduction of Cu(II) in FAU matrices at different reduction temperatures (a – XANES, b – modulus of Fourier-transformed k^2-weighted EXAFS function). The spectra of *all* initial samples and of the final reduction products are collected in Figure 5. The term "initial" refers to samples that had been heated in flowing He to 390 K at 5 K/min and dried at this temperature for 15 min.

From the initial EXAFS spectrum in Fig. 3b, it can be concluded the Cu oxide clusters present in DA-Y are very small although the comparison with other initial spectra (Fig. 5a) implies that the aggregation degree of copper is largest just in this sample. In Fig. 3a it can be seen that during reduction the pre-edge feature indicative of Cu(I) (see arrow) emerges already at 445 K and is very pronounced over a wide temperature range. In EXAFS, the second scattering signal (Cu-Cu at a distance as in CuO) fades away at low temperatures (Fig. 3b). However, already at 515 K, a weak but significant scattering feature at the first distance of Cu metal appears. It grows moderately but remains small upon further temperature increase by ≈50 K. As this is just the temperature region where XANES indicates the predominance of Cu(I), we have to conclude that Cu ions and Cu metal nuclei coexist in an extended temperature range. Above 590 K, the Cu(0)-Cu

coordination in EXAFS grows significantly and the shape of the XANES approaches that of Cu metal. However, even at the highest reduction temperature (650 K), the Cu(0)-Cu coordination remains much smaller than in the Cu foil, which is given in Fig. 3b for comparison. The higher scattering events are weak and not well separated, and the XANES features typical of Cu metal remain washed out (Fig. 3a). These observations are very similar to those made with Cu(II) in silicalite-1[9], where, however, the temperature range of coexistence between Cu(I) and Cu(0) nuclei was even more extended.

With CuNa-Y(C), the course of the reduction is entirely different (Fig. 4). There are hardly any changes in the XANES up to 480 K where Cu-DAY is already reduced to an appreciable extent (compare to Fig. 3a). At higher temperatures, the edge shifts to lower energy and gradually adopts a complicated shape characterized by three inflection points (Fig, 4a, spectra between 595 and 810 K). In EXAFS (Fig. 4b), no feature that would indicate the presence of Cu(0) appears below 750 K. The first coordination sphere (O) decreases with increasing reduction temperature. The second sphere, which is usually assigned to Cu neighbours in Cu oxide clusters, is extremely small in the initial sample (see also Fig. 5a), but increases strongly upon reduction and remains intense up to high temperatures. Above 810 K, a Cu(0)-Cu coordination emerges. At 865 K, it is still much weaker than in the other samples (Fig. 5b), but scattering signals from the higher Cu metal coordinations are already visible. The considerable width of the scattering feature peaking at 2.15 Å shows that there are still significant contributions both of the first and the second coordination sphere typical of Cu ions in this sample. Accordingly, the XANES is still more characteristic of the ionic state (though washed out) than of Cu metal (Fig. 4a).

The spectra measured during the reduction of the remaining samples may be well described by reference to those depicted in Figs. 3-5. The series taken with CuNa-Y(D) has been earlier shown in[13]. In the initial CuNa-Y(D) (Fig. 5a) EXAFS indicates very low order beyond the first (Cu-O) shell. In the reduction series, the spectra obtained at low temperatures resemble those of CuNa-Y(C) (cf. Fig. 4): the scattering intensity around 2.5 Å (uncorrected) increases markedly

when the temperature is raised to 495 K whereas the edge position (XANES) remains constant up to 485 K and indicates beginning reduction only at 495 K. Already at 510 K, however, a contribution of Cu(0) (≈ 2.15 Å, uncorrected) emerges and grows strongly upon moderate temperature increase. In Fig. 5b, where the Cu*K* EXAFS spectra of the final reduction products are compared, it can be seen that unlike Cu metal produced in the DA-Y matrix, the metal aggregates formed in the uncalcined Y zeolite exhibit intense and well separated scattering features between 3 and 8 Å (uncorrected) already after reduction at 570 K. A slight asymmetry of the first Cu(0)-Cu scattering feature to lower distances may indicate the presence of residual Cu ions.

In the zinc containing materials, the copper dispersion in the initial state is similar as in the samples without zinc (Fig. 5a): From the intensity of the second shell at ca. 2.5 Å (uncorrected) one can judge that the cluster size is somewhat smaller in ZnCu-DAY than in Cu-DAY whereas there is no significant difference between the materials made with Y zeolite. The Zn*K* spectra (Fig. 6) imply that the short-range order around zinc is far from that in ZnO. In the initial ZnCu-Y, no long-range order beyond the first (O) neighbour can be seen at all. There is a weak higher shell in ZnCu-DAY, but as opposed to the Cu species (Fig. 5a), the higher shell in ZnCu-DAY appears at a distance significantly different from that in the bulk oxide (2.72 Å *vs.* 2.86 Å (uncorrected) in ZnO), i.e., there are no oxide clusters with ZnO short-range order.

The reduction of ZnCu-DAY will be described by reference to that of Cu-DAY (Fig. 3). In the zinc-containing sample, hardly any changes appear up to 485 K where Cu(I) is already clearly observed in Cu-DAY (cf. Fig. 3a). In ZnCu-DAY, the XANES signature of Cu(I) emerges at 515 K but is never as pronounced as in absence of zinc. The Cu(0)-Cu shell can be seen at 535 K, but only at 650 K, the reduction appears to be complete (see spectrum in Fig. 5b). In this higher temperature region, the course of reduction largely parallels that observed with Cu-DAY.

The reduction of ZnCu-Y resembles that of CuNa-Y(D) rather than of CuNa-Y(C) although the zinc-containing sample had been calcined. After only minor changes up to 485 K, an edge shift indicates the beginning Cu(I) formation at 525K. At 535K, the Cu(0)-Cu path at 2.15 Å (uncor-

rected) appears very weakly, but already at 565 K, the metal signal is fully developed though with a shoulder indicating residual Cu ions. This shoulder disappears gradually at higher reduction temperatures while the main Cu(0)-Cu coordination grows only marginally to result in the spectrum for 650 K shown in Fig. 5b. In this spectrum, the signals of the higher shells are not separated at all. It should be noted, however, that with zinc-containing samples, the k range on which the Fourier transformation was based is shorter than with the Zn-free catalysts due to the neighbouring Zn*K* edge. To allow a comparison, the spectrum of CuNa-Y(D) obtained from the same k window is added on top, which confirms the observation of less separation between shells in the zinc-containing samples as compared to CuNa-Y(D).

The composition of mixtures (in our case – Cu(II), Cu(I), and Cu(0)) is usually determined by analyzing the contributions of the components to the XANES region. This approach is appropriate only if the XANES of the components are invariable throughout the series of mixtures. Unfortunately, this does not apply to our case because with highly disperse metal particles, the XANES depends on the degree of dispersion[23], which is also illustrated by our own data (compare Cu obtained by reduction of Cu-DAY and in the foil, Fig. 3a). Analogously, the XANES of our initial Cu(II) species differs from that of CuO and shows subtle differences between samples. Therefore the invariability of the component contribution is under doubt for all components. Indeed, in attempts to assess Cu(II), Cu(I) and Cu(0) percentages in reduced Cu-DAY on this basis, the Cu(0) contributions at intermediate temperatures, which are clearly proven in the EXAFS (Fig. 3b), could not be extracted from the XANES. As introduced previously[9], we have therefore extracted indirect information about the species distribution by decomposing the first shell in EXAFS into three contributions indicative of Cu(II), Cu(I), and Cu(0) (Cu-O for Cu(II) restricted to 1.94 Å < r < 1.97 Å, Cu-O for Cu(I) restricted to 1.84 Å < r < 1.87 Å, Cu(0)-Cu free). Where necessary, a fourth shell (Cu-Cu at 2.87-2.91 Å) was included to represent remaining oxide clusters. It should be noted that this analysis considers the Cu ions to be part of a Cu oxide structure and is likely to fail with alumosilicate FAU where the coordination geometry imposed

by the zeolite lattice should determine the Cu-O distances (cf. [24-27]). It has been, however, successfully applied to the reduction of an overexchanged Cu-ZSM-5 (Cu/Al ≈ 0.45)[9] Notably, coordination numbers (C.N.) cannot directly reflect the concentration of a species in the mixture because the C.N. of a given phase are primarily related to degrees of aggregation. However, when the species compared are in high, comparable dispersion, the trends of the C.N. should qualitatively reflect the abundance of the species.

The coordination numbers obtained by such fits are reported in Figures 7 and 8 in the form of "normalised coordination numbers" obtained by dividing the observed C.N. by those known from the respective bulk phases (CuO - 4, Cu_2O - 2, Cu metal - 12). Fig. 7 shows the data for samples made with the dealuminated Y zeolite. In the zinc-free sample (Fig. 7a), the normalised Cu(II)-O C.N. first decreases without reduction products being detectable. We ascribe this to dehydration phenomena in the samples that had been stored in air after calcinations (where applied) and only dried at 390 K for the study of the initial state. As deduced above there is a broad temperature range during reduction of Cu-DAY where Cu(I) and Cu(0) coexist, with hardly any change of the Cu(I) normalised C.N. A rapid reduction of the residual Cu ions is not induced by the zerovalent copper (Fig. 7a). Fig. 7b shows that zinc strongly retards the onset of Cu(II) reduction. In ZnCu-DAY, the temperature range of coexisting Cu(I) and Cu(0) is narrower than in Cu-DAY. Above 550 K, the catalyst state becomes very similar in both samples. This is in perfect agreement with the TPR profiles (Fig. 2) where the reduction rate peaks at higher temperature with ZnCu-DAY whereas the pronounced tailing of the signal tends to a coincidence with that of the second maximum in the zinc-free sample.

Plots of the normalised C.N. *vs*. temperature for the materials prepared from Y zeolite are given in Fig. 8. In these samples, indications for Cu-O contributions at ≈1.86 Å have been found only in exceptional cases (ZnCu-Y reduced at 535 K, CuNa-Y(C) at temperatures above 750 K (Fig. 8c, b) although the obvious shifts in the XANES at 500 - 550 K (cf. Fig. 4a) prove the reduction of Cu/II) to Cu(I). Given the not unexpected failure of our approach to distinguish Cu ions in Y,

the coordination number of the next O atoms at ≈1.96 Å was normalized to $(C.N.)_0 = 4$ in Fig. 8, and the predominance of Cu(II) or Cu(I) as derived from the edge position was indicated by shading the data points.

As seen in the TPR curves, the reduction of Cu(II) sets on at much higher temperatures in Y than in DA-Y (Figs 2, 7a, 8a): Cu(I) formation was seen at 445 K with the latter, but at 495 K in CuNa-Y(D) and only at 540 K with CuNa-Y(C). On the other hand, the onset of Cu(0) formation occurs in the same temperature region in Cu-DAY and in CuNa-Y(D). In the alumosilicate matrix, however, the Cu(0)-Cu normalised C.N. grows more rapidly once the first nuclei have been formed (Fig. 8a). As indicated above, calcination of CuNa-Y changes the reduction behaviour dramatically (Fig. 8b). The influence of zinc is different in the siliceous and the alumosilicate FAU: In DA-Y, it clearly retards the reduction of Cu(II) while in Y it has the effect that the calcined sample (i.e. ZnCu-Y) behaves like the uncalcined CuNa-Y(D) (as opposed to CuNa-Y(C)). In ZnCu-Y the particularly steep increase of the normalized Cu(0) C.N. between 535 and 565 K apparently reflects the pronounced autocatalytic rate maximum in the TPR profile (Fig. 2).

Although the Zn*K* spectra (Fig. 6) exhibit much less changes during reduction than the Cu*K* spectra, some interesting observations can be made. As mentioned above, all spectra differ strongly from that of ZnO, which is expected for ZnCu-Y, but not a priori for ZnCu-DAY. There, the XANES is almost completely featureless and resembles that found in zinc-modified mesoporous siliceous M41S phases[12]. Upon reduction, a small shift of the second scattering event (2.7 Å, uncorrected) to lower distances is seen in EXAFS, which is, however too small to allow reliable conclusions to be drawn from model calculations. A significant reduction of Zn(II) can be excluded because there are no changes in the XANES, and it is doubtful that the shift seen in EXAFS could arise from nearby Cu(0).

In ZnCu-Y, the second EXAFS coordination sphere, which is completely absent in the initial sample, develops upon reduction of the sample as previously seen in the Cu*K* EXAFS spectra of CuNa-Y(C) (Fig. 4b). There is, however, no evidence of Zn(II) reduction neither in the EXAFS

nor in the XANES. Notably, significant changes of the XANES shape occur in this sample: Upon reduction, the principal maximum becomes weaker, and a clear shoulder emerges at an energy where ZnO exhibits a maximum. Due to the complicated theory of the XANES region, it is, however, difficult to relate these changes to definite structural modifications.

Discussion

In the initial samples, the transition-metal ions are well distributed over the porous matrices. This can be concluded from surface analysis (surface and bulk Me/Si atomic ratios (Table 1), Cu Auger spectra and the Cu Auger parameters (Fig. 1, Table 1)) as well as from EXAFS (Fig. 5a, 6b). In no case, bulk oxide phases can be observed. In the fully exchanged ZnCu-Y (according to $Me^{2+}/Al = 0.5$), the considerable surface enrichment of Cu, but also of Zn (Table 1) indicates an overexchange near the external surface. However, since EXAFS does no suggest significant aggregate formation (Fig. 6b, 5a; the Cu spectrum is similar to that of CuNa-Y(D), with 1.6 wt-% Cu), we suggest that the excess ions are exchanged together with extra-lattice oxygen (i.e. as $Me(OH)^{+}$). In the siliceous DA-Y matrix, the formation of very small Cu oxide clusters is obvious from the EXAFS spectra (Fig. 5a). In all initial samples, the Cu-O distances (fitted without constraint) were ≈1.96 Å, and the C.N. were near 4. The Cu-O distances reported for Cu(II)-Y in earlier studies range from 1.96 to 2.01 Å [24-27].

In the reduction study, the results from the (instationary) TPR technique and from the (stationary) reduction runs analysed by XAFS are on the whole well in agreement. The reduction starts at the lowest temperature with Cu-DAY (Figs. 3, 7) and extends to the highest temperature with CuNa-Y(C) (Fig. 4). Cu(II) is reduced at higher temperatures in the polar FAU matrix than in the dealuminated one, and the reduction is also delayed by the presence of Zn in DA-Y.

The results obtained with siliceous FAU and (uncalcined) alumosilicate FAU are related to each other in a similar way as those described in [9] for siliceous and alumosilicate MFI. XAFS shows that both Cu(I) and some Cu(0) are formed readily in the two siliceous matrices and coexist over

a wide temperature range with only moderate increase of the Cu(0)-Cu normalised C.N., until the reduction rate increases again at high temperature (see Fig. 7 for Cu-DAY). This reflects the two-step reduction process observed in TPR (Fig. 2), however, with metal nuclei present already in the rate minimum between the two TPR peaks. With CuNa-Y(D), XAFS sees the majority of Cu ions converted to the metal in the same temperature range as in the non-polar DA-Y matrix whreas the reduction of the initial Cu(II) starts at significantly higher temperature in the alumosilicate FAU. Such higher temperature of Cu(II) reduction onset is apparently a consequence of the electrostatic stabilisation of the cations by the polar alumosilicate matrix, because it was not found with the high-silica ZSM-5 zeolite[9]. Given the obvious stabilisation of charged particles by the Y matrix, it is unexpected to see the formation of the uncharged Cu metal in the same temperature range in siliceous and alumosilicate FAU.

The case of the calcined CuNa-Y(C) is particular. It is well known that multiply-charged cations tend to occupy remote sites of the FAU structure (S_I, $S_{I'}$, $S_{II'}$) where they experience a favorable electrostatic stabilisation[28]. The observation that during reduction of CuNa-Y(C) no trace of Cu(0) can be found up to 750 K strongly suggests that the site exchange of Cu(II) with Na ions to access the remote sites was completely achieved by the thermal treatments applied. However, the stabilisation was much stronger with respect to Cu(I) than with Cu(II) where the upshift of the reduction temperature (relative to CuNa-Y(D)) was just 25 K (seen by TPR) to 50 K (seen by XAFS). This difference may be related to several factors. The remote sites offer a more compact coordination environment, which stabilises Cu(II) as well as Cu(I). From Cu*K* and Zn*K* EXAFS (Fig. 4b, 6b) it may be concluded that the order in these structures increases as the temperature is increased (*vide infra*). In the case of Cu, this applies to the monovalent ion that has already formed under these conditions and experiences, therefore, an extra stabilisation. A different contribution may arise from the lower chance of aggregation for a metal atom formed on a remote site: in the large cavity, the higher probability to stabilise by aggregation with other Cu metal atoms (instead of encountering reverse reaction with zeolite OH groups) may further favour the

reduction pathway. Once metal aggregates above a critical size are formed, the reduction process may be accelerated by hydrogen activated on them[9], which is, however, completely absent in CuNa-Y(C) below 750 K.

As expected, the spectroscopic signature of Cu(I) in Y differs strongly from that of Cu(I) in overexchanged ZSM-5, where the XANES was close to that in Cu_2O and the EXAFS fit rendered a coexistence of Cu-O distances at ≈1.85 and ≈1.96 Å even without constraints [9]. In Y zeolite, the Cu-O distance remains near 1.96 Å in a temperature region where both TPR and XANES (edge shift) suggest that the reduction of Cu(II) has taken place (T > 540 K, Fig. 2, 4). At the same time, a complicated XANES shape appears. In [29], XANES shapes of 40 Cu compounds are compiled, but none of them corresponds to the shape observed during the reduction of CuNa-Y(C), in particular in the 700-800 K temperature range (Fig. 4a). XANES spectra of Cu(I) in Y have been shown earlier in [24-26,30]. A well-separated pre-edge peak was found for Cu(I)-Y of high exchange degree in [24,25]. Opposed to this, Yamashita et al. [26] reported a shape reminiscent of the spectra in Fig. 4a for Cu(II)-Y evacuated at 973 K but assign the structure to a mixture of Cu(I) and Cu(II). In our samples, edge-shift and TPR data render the presence of Cu(II) at the temperature of beginning Cu(0) formation (750 – 810 K) highly unlikely. Hence, the structure is probably caused by Cu(I) ions in different coordination geometries. It is obvious from [29] that the edge *position* of Cu(I) compounds is quite insensitive to coordination sphere and even ligand identity. Hence, the two shoulders at 8983 and 8989 eV (arrows in Fig. 4a) must not be considered as separate edge steps caused by two sites present. The major edge features of the Cu*K* XANES arise from 1s-4p transitions, the splitting between $4p_z$ and $4p_{xy}$ exerting a pronounced influence on the signal shape. Hence, the structure observed may arise from Cu sites with very different ligand symmetry and, hence, different splitting between $4p_z$ and $4p_{xy}$. It would be an interesting and challenging task to assign these sites by studying the development in

the XANES in a series of CuNa-Y with different Cu ion distributions over the sites, which would have to be analysed by an independent technique, e.g. XRD.

It should be noted that the influence of the matrix on the Cu(I) signature holds also for CuNa-Y(D) and ZnCu-Y where the sample history and the reduction behaviour suggest that almost all Cu ions occupy sites in the large cavity although some might have managed to escape to remote positions in CuNa-Y(D) during the reduction runs. Opposed to this, reduction caused the Cu-O signal in Cu-ZSM-5 to shift to distances that allow for a large contribution of a Cu(I) component fixed between 1.84 and 1.87 Å[9]. This is different from some other reports where Cu(I)-O distances equal to or even larger than Cu(II)-O have been observed for Cu-ZSM-5 of different preparation (e.g. solid-state ion exchange with CuCl)[31,32]. It has been found earlier that the aqueous exchange via copper acetate solution leads to surface enrichment and formation of oligomeric clusters in the MFI matrix [8], and the material studied here exhibited a different reduction behaviour than reported in other sources (cf. [9] and literature cited there). Apparently, when overexchange is targeted with aqueous solutions of Cu salts, the ZSM-5 behaves as a siliceous rather than as an alumosilicate matrix: The Al present introduces hydrophilic properties which helps to introduce copper species into the pore system in large amounts (over-exchange phenomena). However, even at moderate degrees of over-exchange, most Cu species behave like oxide nanoclusters during reduction.

A notable feature of the EXAFS spectra of Cu and Zn ions in Y zeolite is the significant growth of the second coordination sphere with increasing reduction temperature. This is most obvious with CuNa-Y(C) (Fig. 4b), but can also be observed in the Zn*K* spectra of ZnCu-Y (Fig. 6b) and even with CuNa-Y(D) up to the temperature of Cu metal formation (not shown). A possible explanation is that these signals arise from (initially disordered) oxide clusters as has been discussed in an earlier study on solid-state ion exchange of NH_4-Y with $NiCl_2$, CuCl, or $ZnCl_2$ [30]. However, given the straightforward reduction both of extra-zeolite CuO and of Cu(II) in the

large cavity of Y (cf. CuNa-Y(D)), we can safely exclude this situation for copper in CuNa-Y(C), and we believe the zinc case to be similar. The trend to higher (or different) order upon heat treatment may also arise from cation migration, e.g. upon reduction of Cu(II) to Cu(I). However, in CuNa-Y(C), the higher shells increase already at T≤480 K where reduction is negligible (Fig. 5b), and the same phenomenon occurs in the spectra of the irreducible Zn ions (Fig. 6b). We believe therefore that the growth of the second coordination sphere with increasing reduction temperature reflects that the transition-metal ions are not well ordered in the Y structure as long as they are not fully dehydrated.

It was attempted to analyse the average coordination sphere of the Cu ions in CuNa-Y(C) from representative spectra (after reduction at 485 and 595 K). Examples for the fits are given in Fig. 9, the model parameters are summarized in Table 2. Considering these data, it should be noted that in the analysis of the second shell (between 2.3 and 3.2 Å, uncorrected) it is possible to obtain good fits with a great number of models that do not bear chemical sense: When using different scatterers (O, Al, Si, Cu) many geometries may result in partially destructive interference to reproduce the relatively weak signal in the spectrum. However, any solution with realistic coordination numbers invariably involved also Cu neighbours, i.e., the presence of Cu in the second Cu coordination sphere is very likely. Indeed, in [26], a similar spectrum was analyzed with a Cu-Cu shell, however at an unrealistic C.N. of 6. In single-shell fits, the first (O) coordination number tended to a value of 4 (Table 2).

The fits presented in Fig. 9 and Table 2 have been obtained with constraints derived from a model in which S_I and $S_{I'}$ sites are occupied. It has been argued that adjacent S_I and $S_{I'}$ sites are not likely to be occupied for electrostatic reasons [24]. However, such situation, in which the monovalent cations are shielded by the six-ring oxygens, could well explain the Cu-Cu distances found in the fits (slightly above 3 Å, cf. Table 2) as well as the C.N. of 4 obtained for the nearest O shell (6 for S_I, 3 for the two $S_{I'}$ sites). An alternative explanation for Cu-Cu coordinations observed could be a coexistence (in each sodalite cage) of more than 2 Cu ions in I* sites (center of

six-membered ring of hexagonal prism [24]). The constraint used for the fits presented here has been derived from the former model (average C.N. of 8 for the sum of T atoms (Al, Si) - 12 for S_I, 6 for the two $S_{I'}$ sites). With one $S_{I'}$ -S_I - $S_{I'}$ string, the Cu-Cu C.N. will tend to 1.33 (2 for S_I, 1 for the two $S_{I'}$ sites), but larger C.N. might be explained by including more than one $S_{I'}$ site per sodalite cage because the distance between two $S_{I'}$ positions in the sodalite cage should be similar. The models neglect possibly present Na ions and asymmetric cation positions that might arise from asymmetric Al distributions in the six-rings. In the models of type A, the Cu-Si and Cu-Al distances and Debye-Waller factors were kept identical and a C.N. of 2 was set for the Cu-Cu scattering path. Releasing these constraints (models B) led to significant improvements, but for the sample reduced at 595 K, the Cu-Cu C.N. tended towards the upper limit set (3.0). While the higher degree of ordering among Cu ions, which is indicated by this result, may reflect a real effect, the significance of the models obtained should not be overemphasized. Given the large number of parameters and ill-specified constraints, they may serve to illustrate that plausible situations may be reflected in the data, but not to prove any structure hypothesis.

A comparison of Cu*K* EXAFS spectra measured after reduction of Cu(II) in different matrices (Fig. 5b; CuNa-Y(C) omitted because complete reduction was not achieved) shows that different products have been formed. The spectrum of CuNa-Y(D) differs from the remaining ones in a pronounced separation between the higher scattering features (3-5 Å (uncorrected)) and in a larger first Cu-Cu distance (Fig. 5b), which is similar as in the spectrum of the Cu foil. The first Cu-Cu C.N. is, however, much smaller in the reduced Y sample (5.6 *vs*. 12). Based on a geometrical correlation derived in [33], a C.N. of 5.6 corresponds to an average particle diameter of 8-9 Å (spherical shape assumed), which is obviously at variance with the pronounced scattering from distances between 6 and 8 Å (uncorrected) and the lack of amplitude decay between 3 and 5 Å (uncorrected)). Therefore, though dominated by the contribution of very large particles, the spectrum indicates the simultaneous presence of a significant minority of very small entities

(probably oligomers because they affect only the first shell). Their existence may be favoured by the relative low reduction temperature at which this series was finished (570 K).

With Cu-DAY and ZnCu-DAY (both reduced at 650 K, Fig. 5b), the C.N. of the first Cu-Cu shell (6.9 and 7.8, respectively, *vs.* 5.6) indicates a somewhat larger average particle size than in CuNa-Y(D) (10 Å and 11.5 Å, respectively, *vs.* 8.5 Å), but the intensity of the higher shells is smaller than in the latter. Remarkably, the higher shells are least intense with the reduced ZnCu-DAY where scattering beyond 6 Å (uncorrected) is insignificant. This sample appears to have the most homogeneous particle size distribution, the average size of 11.5 Å being well compatible with the size of the large cavity in FAU. Notably, the first Cu-Cu distance found here is significantly below that extracted from the spectrum of the Cu foil (2.51 Å *vs.* 2.543 Å). Such contraction is typical for small metal clusters (see also ref. [9]). For Cu-DAY, the stronger scattering intensity above 6 Å (uncorrected) and the less pronounced amplitude decay between 3 and 5 Å (uncorrected) suggest the presence of larger particles. The reduced ZnCu-Y again combines a small average particle size (C.N. – 5.5, d – 8-9 Å) with significant scattering from high distances (Fig. 5b). Apparently, large particles coexist with smaller ones in this case as well.

The influence of zinc upon the reduction of Cu ions differs for the two matrices studied. In DA-Y, a stabilisation of Cu(II) by the zinc species present is quite obvious from Fig. 7. The particle size distribution of the Cu metal formed was more homogeneous in presence of zinc (Fig. 5b), with the formation of large particles avoided despite the significantly larger copper content of ZnCu-DAY. In Y zeolite, the Zn introduced first occupies the sodalite cages and is apparently not replaced to any significant extent by the copper loaded secondly, despite the final calcination process. Therefore, the reduction behaviour of ZnCu-Y resembles that of the uncalcined CuNa-Y(D) (Fig. 8). However, also in this case, there are strong indications that the presence of zinc retards the formation of large particles (without preventing it completely). This is quite surprising because the reduction, which exhibits the attributes of an autocatalytic step, is much more rapid with ZnCu-Y than with CuNa-Y(D) (Fig. 2), probably because of the higher copper content

in the former. It is hard to conceive how irreducible ions in the remote sites should affect a reduction process in the large cavities. Thus, the effect seems to indicate that there are also Zn ions located in the large cavity in this highly exchanged sample, which contains Zn and Cu in an atomic ratio of ≈2 : 1. The mechanism that keeps the copper better dispersed in presence of zinc remains, however, unclear.

Conclusions

The reduction of Cu(II) species in FAU matrices depends on the composition of the matrices, on the sample history, and on the presence of additional constituents, e.g. zinc ions. In a siliceous FAU matrix, Cu(II) is reduced in two steps, with Cu(0) nuclei already present after the first step. These (oligomeric) nuclei seem to be unable to induce an autocatalytic reduction of the remaining Cu ions. In alumosilicate FAU (Y zeolite), the reduction depends strongly on the sample history, with strong retardation of metal formation caused by previous calcinations of the material (stabilisation in remote cation sites), but straightforward metal formation – accompanied by formation of large, probably extra-zeolite particles – without calcination (sites in the large cavity). The presence of zinc delays the reduction of Cu(II) in siliceous FAU and leads to the formation of smaller Cu particles both in siliceous and alumosilicate FAU.

In Y zeolite, the short-range order around Cu and Zn ions was found to increase upon heating or reducing the samples (by reference to drying at 393 K). The most pronounced order was seen with Cu(I) ions in remote positions, which exhibited a unique XANES signature. Electrostatic stabilisation of Cu ions by the intra-zeolite electrostatic potentials is reflected in an upshift of the Cu(II) reduction temperature relative to the siliceous matrix. No stabilisation was found with ZSM-5 [9] where the intermediate Cu(I) ions exhibited even the spectroscopic signature of Cu(I) in oxide clusters. In Y, the stabilisation led to a moderate upshift of the reduction temperature for positions in the large cavity (80 K in TPR), and an additional slight shift for the remote positions

(25 K in TPR). A strong stabilisation was seen only for Cu(I) in the remote sites were Cu(0) was not formed at all at low temperatures.

Acknowledgements

The work has been funded by the German Science Foundation (DFG) in the framework of the Collaborative Research Center "Metal-substrate Interactions in Heterogeneous Catalysis" (SFB 558), which is gratefully acknowledged. Thanks are due to Mrs. Susanne Wiedemeyer and Mr. Vijay Narkhede for the TPR measurements, and to Dr. I. Ritzkopf (Max-Planck-Institut für Kohlenforschung, Mülheim/Ruhr, Germany) for performing the reaction of DA-Y with diethyl zinc.

References

1 R. Bulanek, B. Wichterlová, Z. Sobalik, and J. Tichy, *Appl. Catal. B*, 2001, **31**, 13.

2 C. Torre-Abreu, C. Henriques, F. R. Ribeiro, G. Delahay, and M. F. Ribeiro, *Catal. Today*, 1999, **54**, 407.

3 C. Torre-Abreu, M. E. Ribeiro, C. Henriques, and G. Delahay, *Appl. Catal. B*, 1997, **14**, 261.

4 M. K. Neylon, C. L. Marshall, and A. J. Kropf, *J. Am. Chem. Soc.*, 2002, **124**, 5457.

5 A. Yamaguchi, T. Shido, Y. Inada, T. Kogure, K. Asakura, M. Nomura, and Y. Iwasawa, *Catal. Lett.*, 2000, **68**, 139.

6 G. Moretti and W. M. H. Sachtler, *J. Catal.*, 1989, **115**, 205.

7 E. S. Shpiro, W. Grünert, R. W. Joyner, and G. N. Baeva, *Catal. Lett.*, 1994, **24**, 159.

8 W. Grünert, N. W. Hayes, R. W. Joyner, E. S. Shpiro, M. R. H. Siddiqui, and G. N. Baeva, *J. Phys. Chem.*, 1994, **98**, 10832.

9 O. P. Tkachenko, K. V. Klementiev, M. W. E. van den Berg, N. Koc, M. Bandyopadhyay, A. Birkner, C. Wöll, H. Gies, and W. Grünert, *J. Phys. Chem. B*, 2005, **109**, 20979.

10 T. R. Oliveira de Souza, S. M. de Oliveira Brito, and H. M. Carvalho Andrade, *Appl. Catal. B*, 1999, **178**, 7.

11 H. Gies, S. Grabowski, M. Bandyopadhyay, W. Grünert, O. P. Tkachenko, K. V. Klementiev, and A. Birkner, *Microporous Mesopor. Mater.*, 2003, **60**, 31.

12 O. P. Tkachenko, K. V. Klementiev, E. Löffler, I. Ritzkopf, F. Schüth, M. Bandyopadhyay, S. Grabowski, H. Gies, V. Hagen, M. Muhler, L. Lu, R. A. Fischer, and W. Grünert, *Phys. Chem. Chem. Phys.*, 2003, **5**, 4325.

13 O. P. Tkachenko, K. V. Klementiev, N. Koc, X. Yu, M. Bandyopadhyay, S. Grabowski, H. Gies, and W. Grünert, *Stud. Surf. Sci. Catal.* 2004, **154***,* 1670.

14 S. Polarz, F. Neues, M. W. E. van den Berg, W. Grünert, and L. Khodeir, *J. Am. Chem. Soc.*, 2005, **127**, 12028.

15 T. Liese and W. Grünert, *J. Catal.*, 1997, **172**, 34.

16 W. Grünert, M. Muhler, K.-P. Schroeder, J. Sauer, and R. Schlögl, *J. Phys. Chem.*, 1994, **98**, 10920.

17 B. A. Sexton, T. D. Smith, and J. V. Sanders, *J. Electron Spectrosc. Relat. Phenom.*, 1985, **35**, 27.

18 I. Jirka, B. Wichterlova, and M. Maryska, *Stud. Surf. Sci. Catal.*, 1991, **69**, 269.

19 J. H. Scofield, *J. Electron Spectrosc. Relat. Phenom.*, 1976, **8**, 129.

20 F. W. H. Kampers, T. M. J. Maas, J. van Grondelle, D. C. Brinkgreve, and D. C. Koningsberger, *Rev. Sci. Instr.*, 1989, **60**, 2635.

21 K. V. Klementiev, *VIPER for Windows (Visual Processing in EXAFS Researches)*, free-ware, www.desy.de/~klmn/viper.html.

22 A. L. Ankudinov, B. Ravel, J. J. Rehr, and S. D. Conradson, *Phys. Rev. B*, 1998, **58**, 7565.

23 D. C. Bazin, D. A. Sayers, and J. J. Rehr, *J. Phys. Chem. B*, 1997, **101**, 1140.

24 G. T. Palomino, S. Bordiga, A. Zecchina, G. L. Marra, C. Lamberti, *J. Phys. Chem. B* 2000, **104**, 8641.

25 C. Lamberti, G. Spoto, D. Scarano, C. Paze, M. Salvalaggio, S. Bordiga, A. Zecchina, G. T. Palomino, F. Dacapito, *Chem. Phys. Lett.* 1997, **269,** 500.

26 H. Yamashita, M. Matsuoka, K. Tsuji, Y. Shioya, M. Anpo, M. Che, *J. Phys. Chem.* 1996, **100**, 397.

27 S. Tanabe, H. Matsumoto, *J. Phys. Chem.* 1990, **94**, 4207.

28 E. F. T. Lee and L. V. C. Rees, *Zeolites*, 1987, **7**, 143.

29 L.-S. Kau, D. J. Spira-Solomon, J. E. Penner-Hahn, K. O. Hodgson, and E. I. Solomon, *J. Am. Chem. Soc.*, 1987, **109**, 6433.

30 H. Förster, and U. Hatje, *Solid State Ionics,* 1997, **101-103**, 425.

31 C. Lamberti, S. Bordiga, M. Salvalaggio, G. Spoto, A. Zecchina, F. Geobaldo, G. Vlaic, M. Bellatreccia, *J. Phys. Chem. B* 1997, **101**, 344.

32 R. Kumashiro, Y. Kuroda, M. Nagao, M. *J. Phys. Chem. B* 1999, **103**, 89.

33 M. Borovski, *J. Phys, IV*, 1997, **7**, C2.

Table 1 - Samples used in the present study – composition (by ICP) and surface-analytical results

Code	Matrix	wt-% metal		Me/Si atomic ratio		$(Me/Si)_{XPS}$		α_{Cu}, eV
		Cu	Zn	Cu	Zn	Cu	Zn	
Cu-DAY	DA-Y	1.1	-	0.010_5	-	0.007	-	1846.9
CuNa-Y(D)	Na-Y	1.6[a]	-	0.022	-	0.018	-	1846.9
CuNa-Y(C)	Na-Y	2.6[a]	-	0.036	-	0.005	-	1846.4
ZnCu-DAY	DA-Y	3.5	6.3	0.037	0.064	0.032	0.054	1846.4
ZnCu-Y	Na-Y	4.9	10.0	0.078	0.155	0.25	0.33	1846.8

[a]exchange degrees (Cu/Al = 0.5) – 11.5 % for CuNa-Y(D) and 18.5 % for CuNa-Y(C)

Table 2 – Model parameters for the simulation of Cu*K* EXAFS spectra measured after reduction of CuNa-Y(C) at 485 K and 595 K (Fig. 9)

Neighbor	r, Å	C.N.	$10^3\ \sigma^2$, Å^{-2}	E_0, eV
reduction at 485 K				
Model A				
O	1.947	4.8	8.1	10.8
Al	2.76	2.4[b]	24.5	17.8
Si	2.76[a]	5.6[b]	24.5[a]	10.8
Cu	3.40	2.0[c]	11.6	3.8
Model B				
O	1.949	4.1	6.4	11.9
Al	2.54	2.4[b]	7.9	20.9
Si	2.70	5.6[b]	10.6	12.0
Cu	3.10	1.3	9.5	19.2
reduction at 595 K				
Model A				
O	1.972	2.7	6.8	11.8
Al	3.12	2.4[b]	17.1	4.8
Si	3.12[a]	5.6[b]	17.1[a]	-2.2
Cu	3.36	2.0c	19.3	4.8
Model B				
O	1.996	4.1_5	11.5	12.1
Al	2.47	2.4[b]	2.6	9.2
Si	2.56	5.6[b]	7.4	-5.1
Cu	2.99	3.0[c]	15.7	16.0

[a]fixed to corresponding value of Cu-Al coordination [b]fixed by Si/Al ratio and fixed sum of both coordinations (8: see text) [c]fixed [d]upper limit

Legends

Figure 1 - X-ray induced Auger spectra of Cu species in FAU matrices (samples described in Table 1).

Figure 2 - TPR profiles of Cu oxide species in FAU matrices, compared with CuO.

Figure 3 - Cu*K* XAFS spectra measured after reduction of Cu-DAY at different temperatures indicated in the figure, comparison with Cu foil. a – XANES, b – EXAFS (Fourier transform (absolute value) of k^2-weighted EXAFS function, 2.7 $Å^{-1}$ < k < 14.7 $Å^{-1}$).

Figure 4 - Cu*K* XAFS spectra measured after reduction of CuNa-Y(C) at different temperatures indicated in the figure, a – XANES, b – EXAFS (Fourier transform (absolute value) of k^2-weighted EXAFS function, 2.7 $Å^{-1}$ < k < 14.7 $Å^{-1}$).

Figure 5 - Comparison of Cu*K* EXAFS spectra in different FAU matrices (Fourier transform (absolute value) of k^2-weighted EXAFS function), a – initial (calcined) samples, 2.7 $Å^{-1}$ < k < 14.7 $Å^{-1}$, b – after reduction at temperatures indicated in the figure. r_{Cu-Cu} (*Å*), determined by fitting of the first coordination shell: Cu foil – 2.543 Å, CuO – 2.54 Å, Cu-DA-Y – 2.53 Å, CuNa-Y(D) – 2.55 Å, CuNa-Y(C) – 2.53 Å, ZnCu-DAY – 2.51Å, ZnCu-Y – 2.53 Å.

Figure 6: Zn*K* XAFS spectra measured after reduction of zinc-containing Cu-FAU samples at different temperatures indicated in the figure, comparison with ZnO and Zn foil. a – XANES, b – EXAFS (Fourier transform (absolute value) of k^2-weighted EXAFS function, 2.4 $Å^{-1}$ < k < 11.9 $Å^{-1}$).

Figure 7: Reduction of copper oxide species in DA-Y (stationary regime, 15 min at temperature T) analysed from EXAFS spectra (fits of the first coordination shell), a – Cu-DAY, b – ZnCu-DAY. Experimental coordination numbers (C.N.) may be obtained by multiplying the normalized C.N. given in the figure with 4, 2, or 12 for Cu(II), Cu(I), and Cu(0), respectively.

Figure 8: Reduction of copper oxide species in Y (static regime, 15 min at temperature T) analysed from EXAFS spectra (fits of the first coordination shell), a – CuNa-Y(D), b – CuNa-Y(C), c – ZnCu-Y. Grey shades in data points indicate Cu(I) as concluded from edge shift. Experimental coordination numbers (C.N.) may be obtained by multiplying the normalized C.N. given in the figure with 4 or 12 for Cu ions and Cu(0), respectively. Grey stars indicate cases where Cu-O distances of ≈1.86 Å were obtained in the fits (see text). The experimental coordination number can be obtained by multiplication with 2 in these cases (cf. Fig. 7).

Figure 9: Model analysis of the Cu*K* EXAFS spectra measured after reduction of CuNa-Y(C) at 485 K and 595 K (parameters in Table 2).

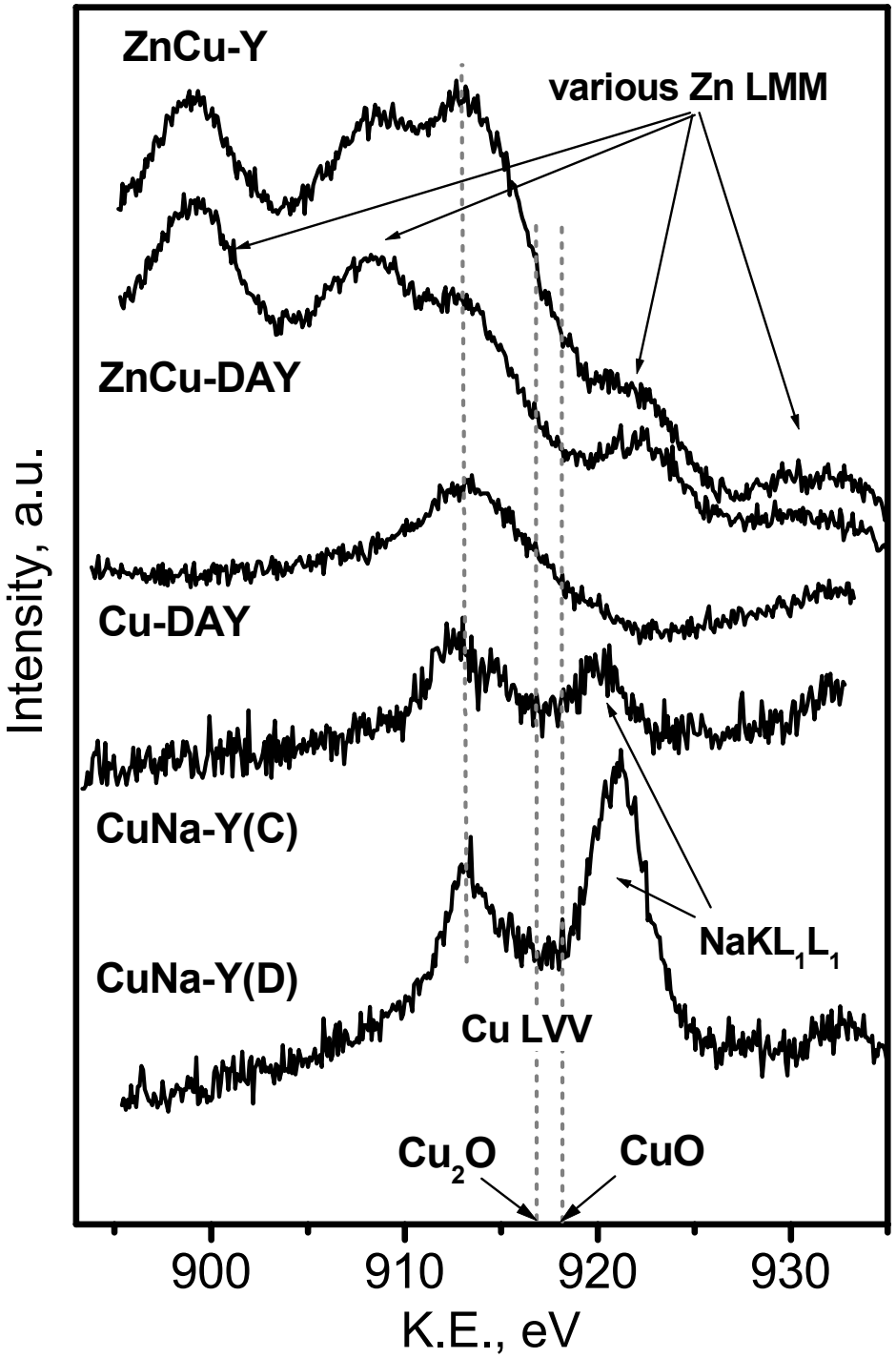
ZnCu-Y
various Zn LMM
ZnCu-DAY
Cu-DAY
CuNa-Y(C)
CuNa-Y(D)
NaKL1L1
Cu LVV
Cu2O
CuO
Intensity, a.u.
900
910
920
930
K.E., eV

Figure 1

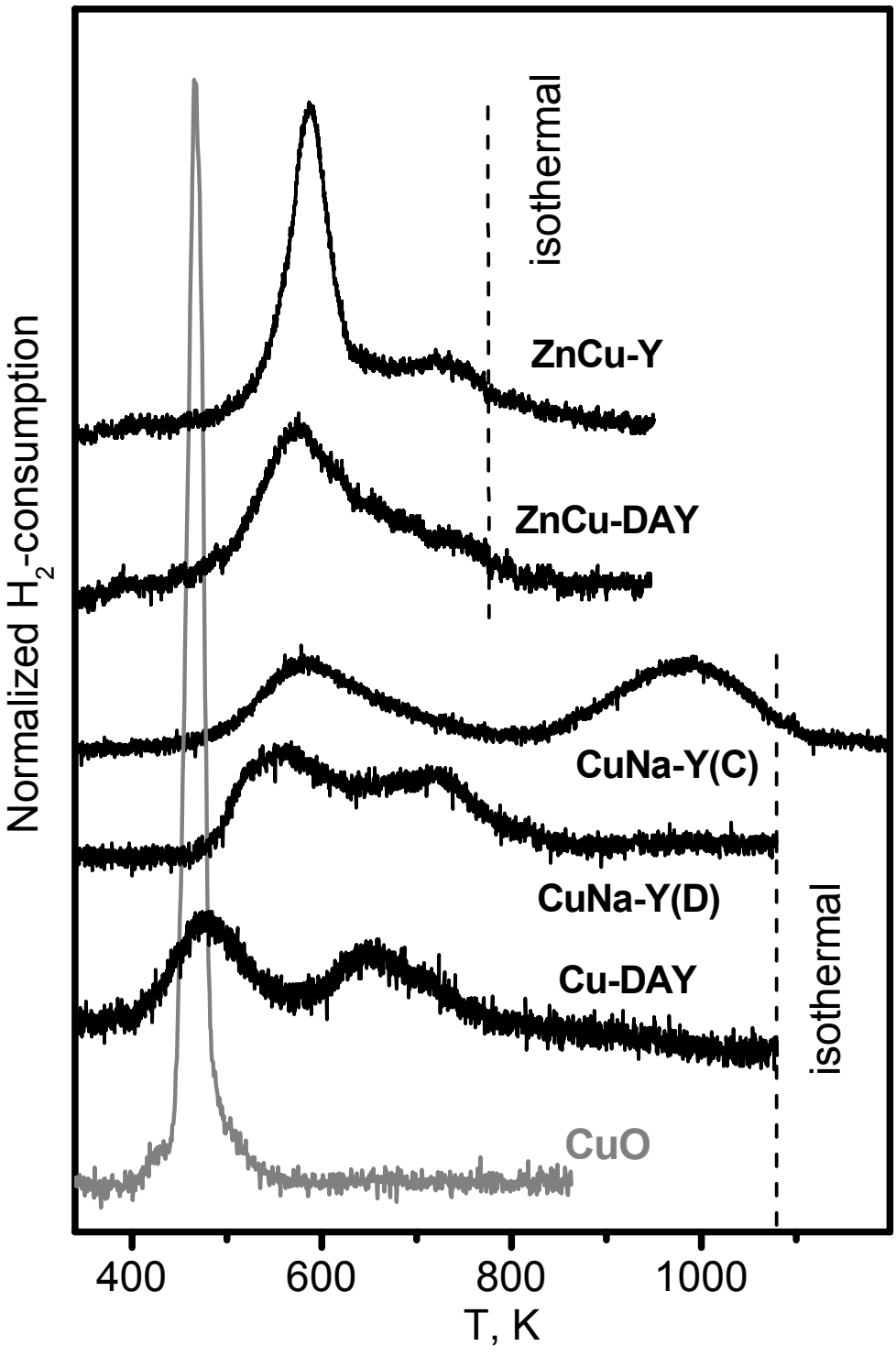
Normalized H_2-consumption
isothermal
ZnCu-Y
ZnCu-DAY
CuNa-Y(C)
CuNa-Y(D)
Cu-DAY
CuO
isothermal
400
600
800
1000
T, K

Fig. 2

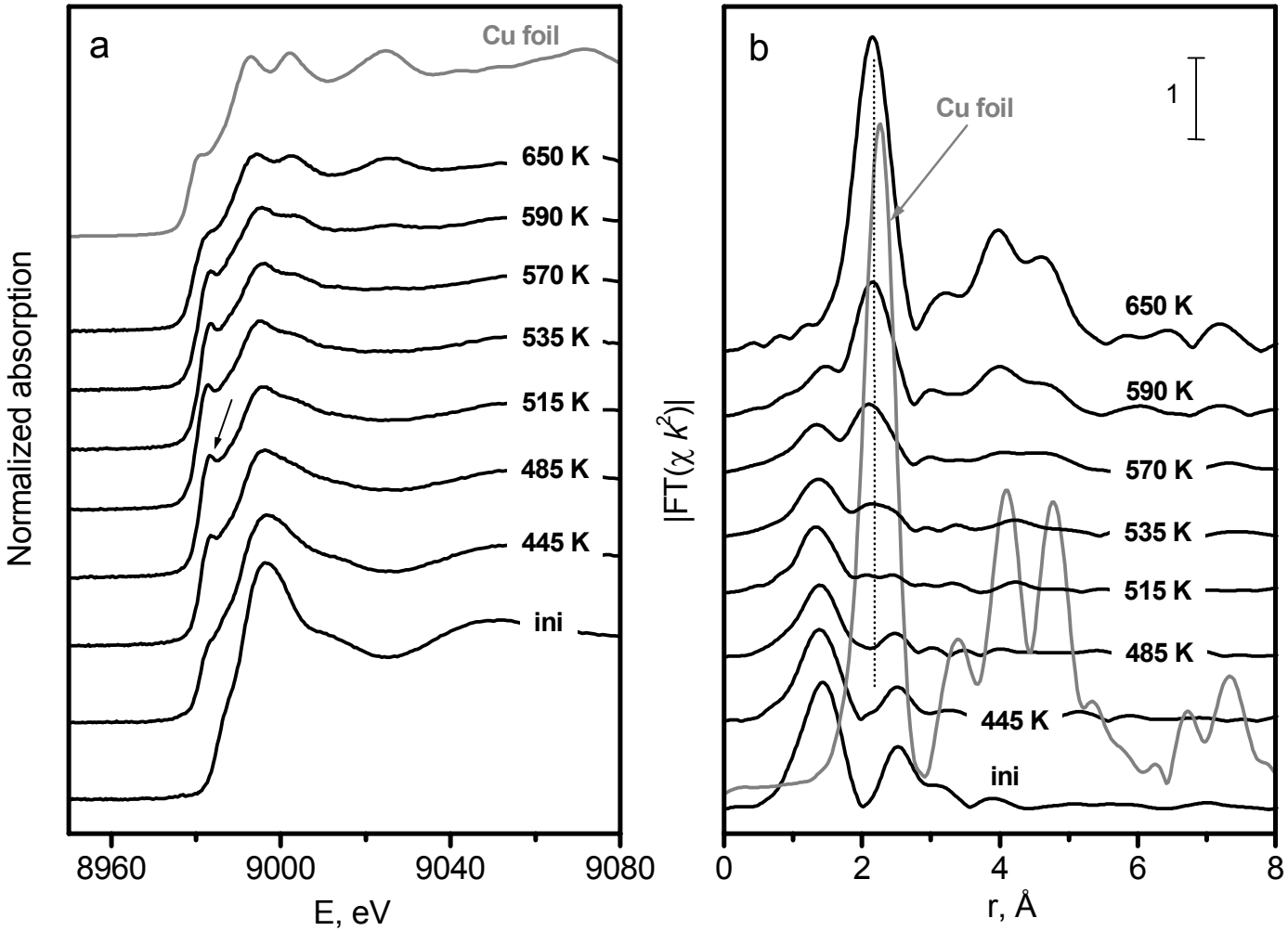
a
Cu foil
650 K
590 K
570 K
535 K
515 K
485 K
445 K
ini
Normalized absorption
8960
9000
9040
9080
E, eV
b
Cu foil
1
650 K
590 K
570 K
535 K
515 K
485 K
445 K
ini
|FT(χ k²)|
0
2
4
6
8
r, Å

Fig. 3

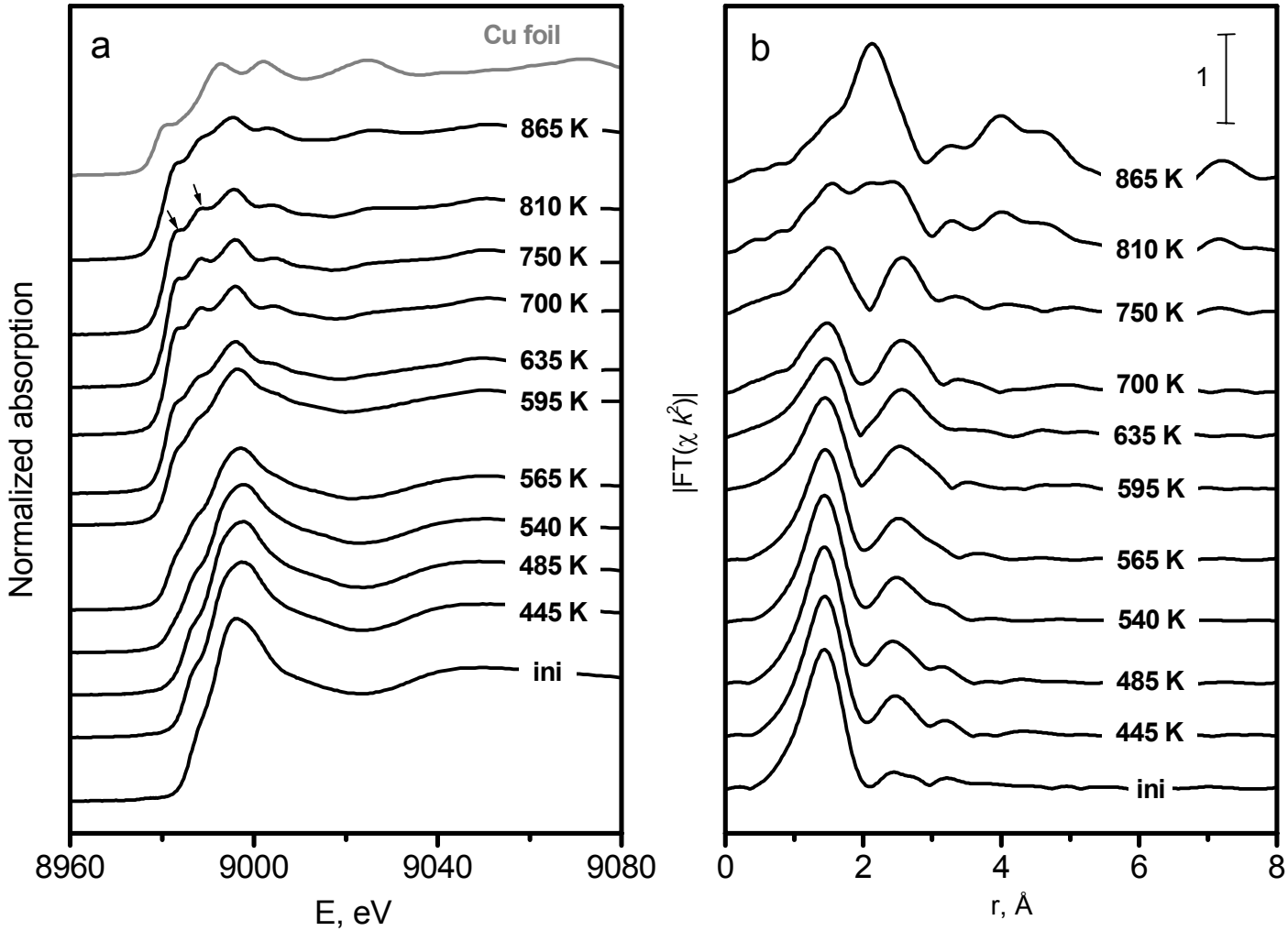
a
Cu foil
865 K
810 K
750 K
700 K
635 K
595 K
565 K
540 K
485 K
445 K
ini
Normalized absorption
8960
9000
9040
9080
E, eV
b
1
865 K
810 K
750 K
700 K
635 K
595 K
565 K
540 K
485 K
445 K
ini
|FT(χ k²)|
0
2
4
6
8
r, Å

Fig. 4

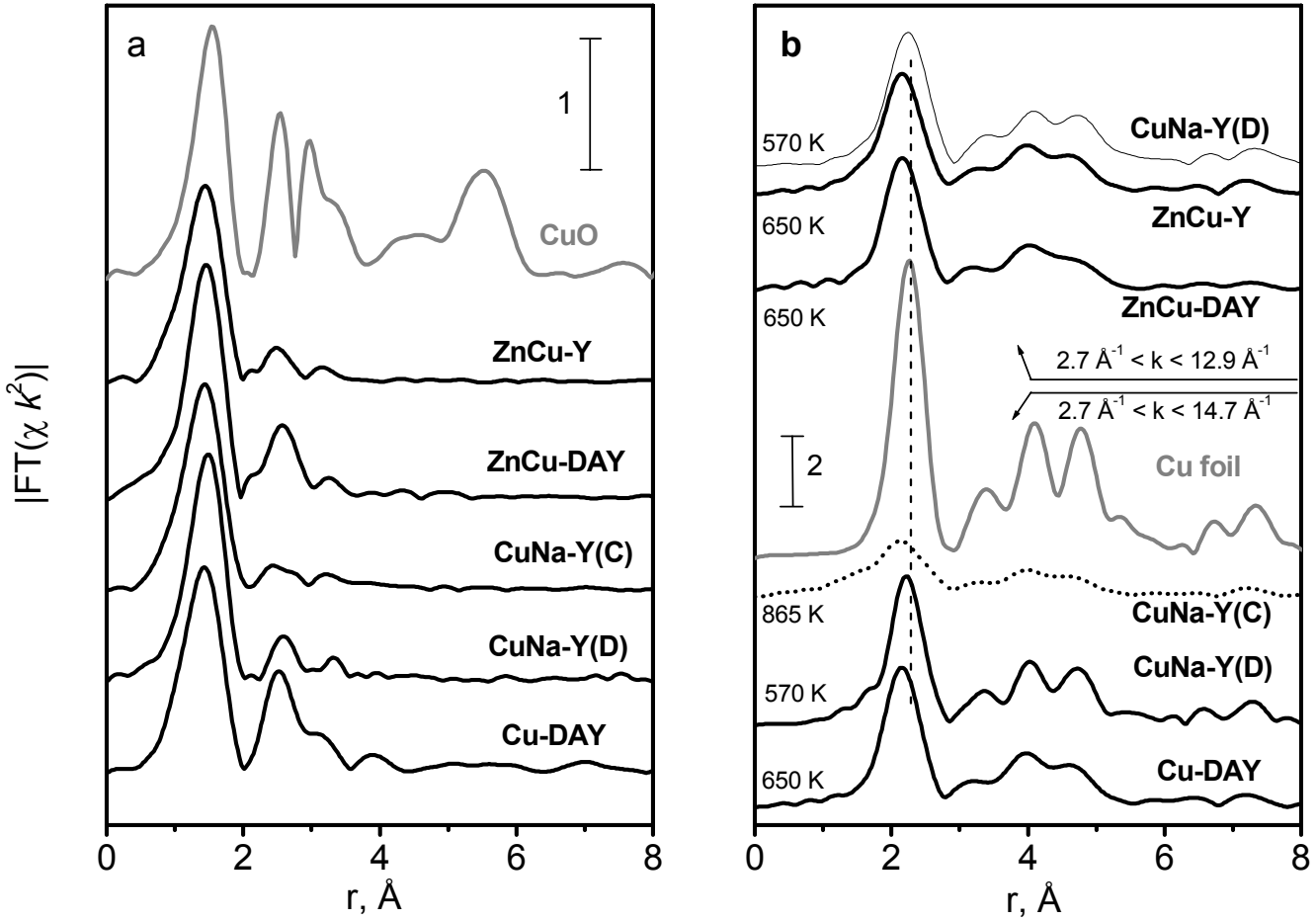
a
1
CuO
ZnCu-Y
ZnCu-DAY
CuNa-Y(C)
CuNa-Y(D)
Cu-DAY
|FT(χ k²)|
0
2
4
6
8
r, Å
b
570 K
CuNa-Y(D)
650 K
ZnCu-Y
650 K
ZnCu-DAY
2.7 Å⁻¹ < k < 12.9 Å⁻¹
2.7 Å⁻¹ < k < 14.7 Å⁻¹
2
Cu foil
865 K
CuNa-Y(C)
570 K
CuNa-Y(D)
650 K
Cu-DAY
0
2
4
6
8
r, Å

Figure 5

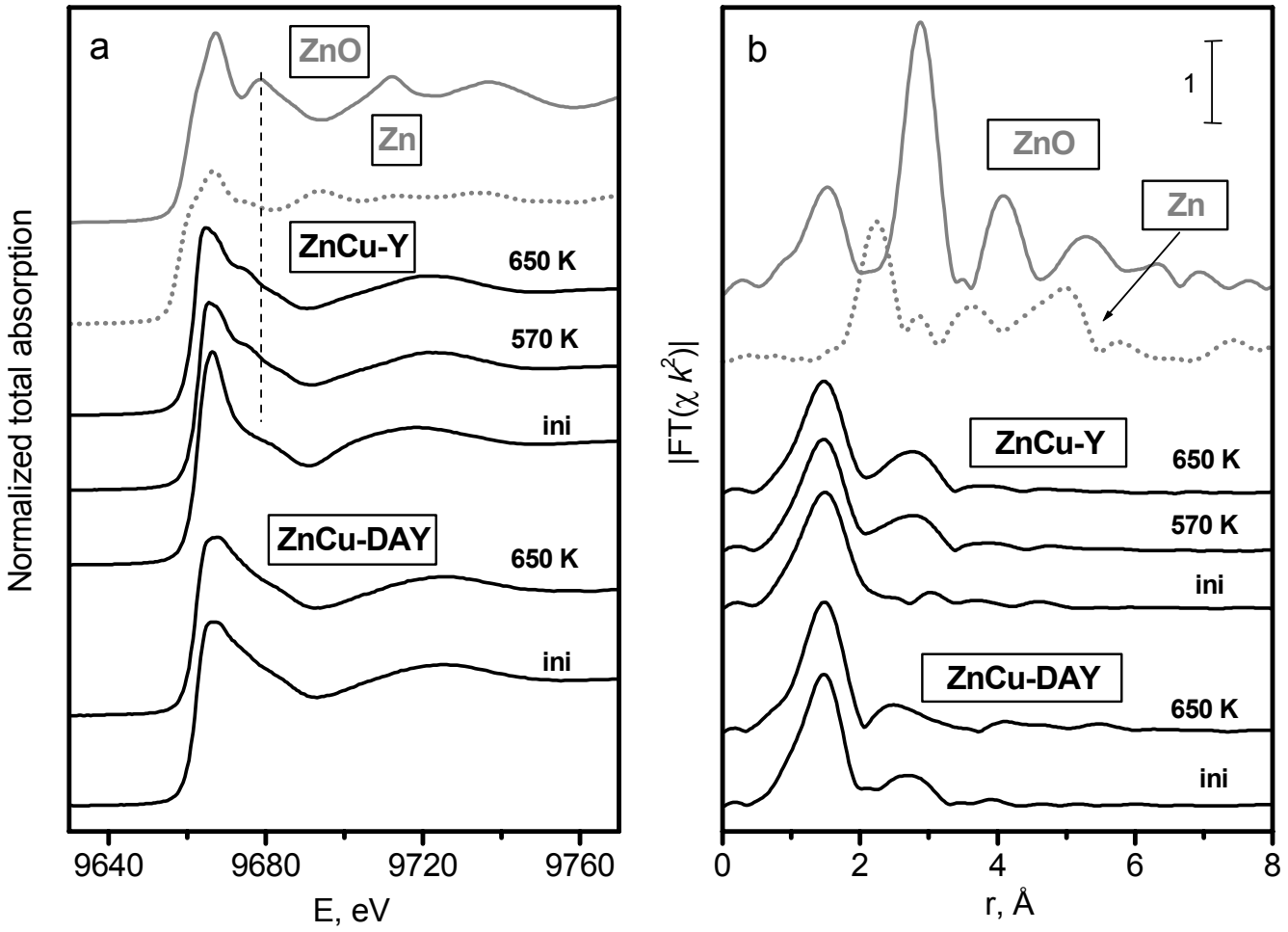
a
ZnO
Zn
ZnCu-Y
650 K
570 K
ini
ZnCu-DAY
650 K
ini
Normalized total absorption
9640
9680
9720
9760
E, eV
b
1
ZnO
Zn
ZnCu-Y
650 K
570 K
ini
ZnCu-DAY
650 K
ini
|FT(χ k²)|
0
2
4
6
8
r, Å

Fig. 6

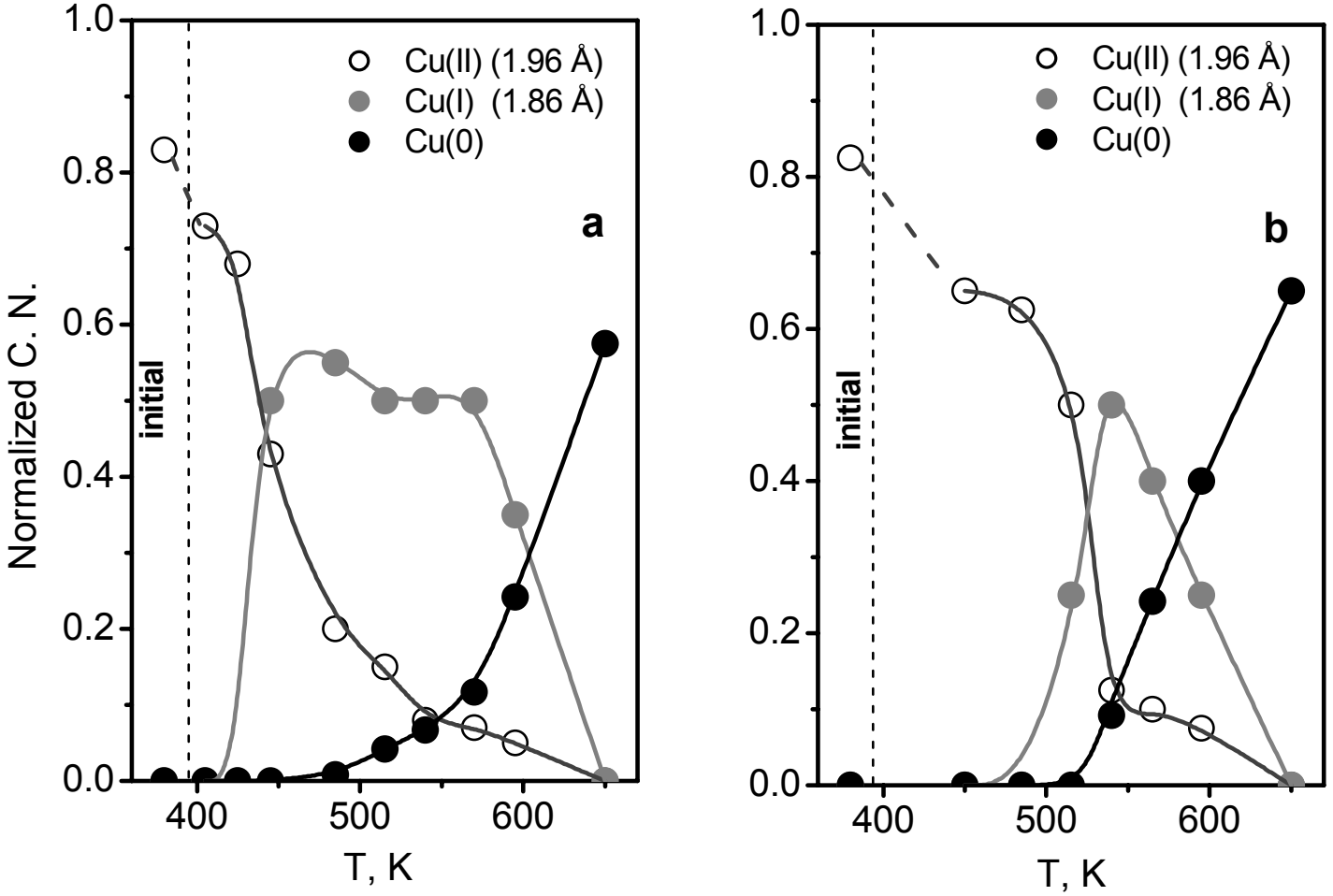
Normalized C. N.
1.0
0.8
0.6
0.4
0.2
0.0
400
500
600
T, K
Cu(II) (1.96 Å)
Cu(I) (1.86 Å)
Cu(0)
initial
a
b

Fig. 7

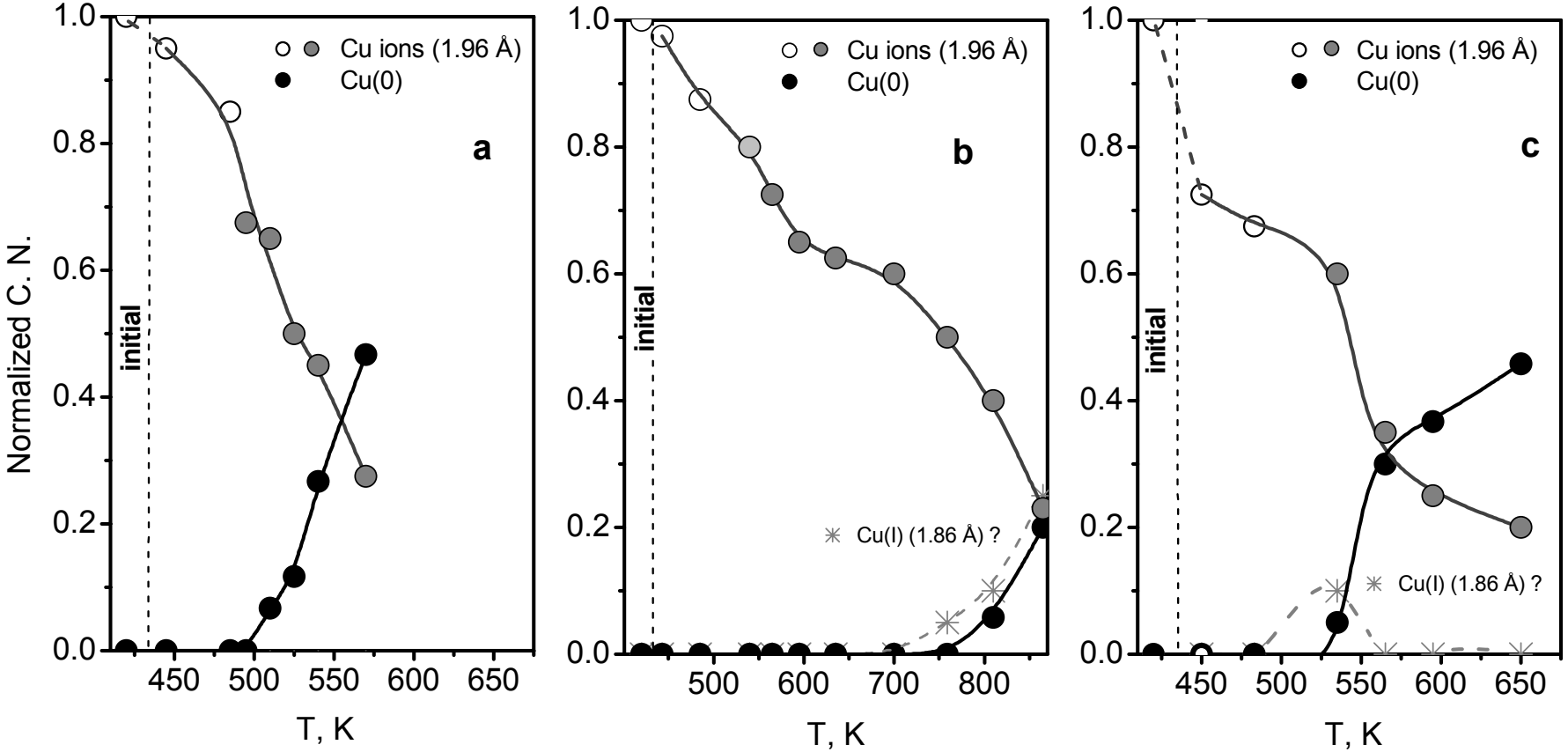
Normalized C. N.
1.0
0.8
0.6
0.4
0.2
0.0
initial
Cu ions (1.96 Å)
Cu(0)
a
450
500
550
600
650
T, K
b
Cu(I) (1.86 Å) ?
700
800
c

Figure 8

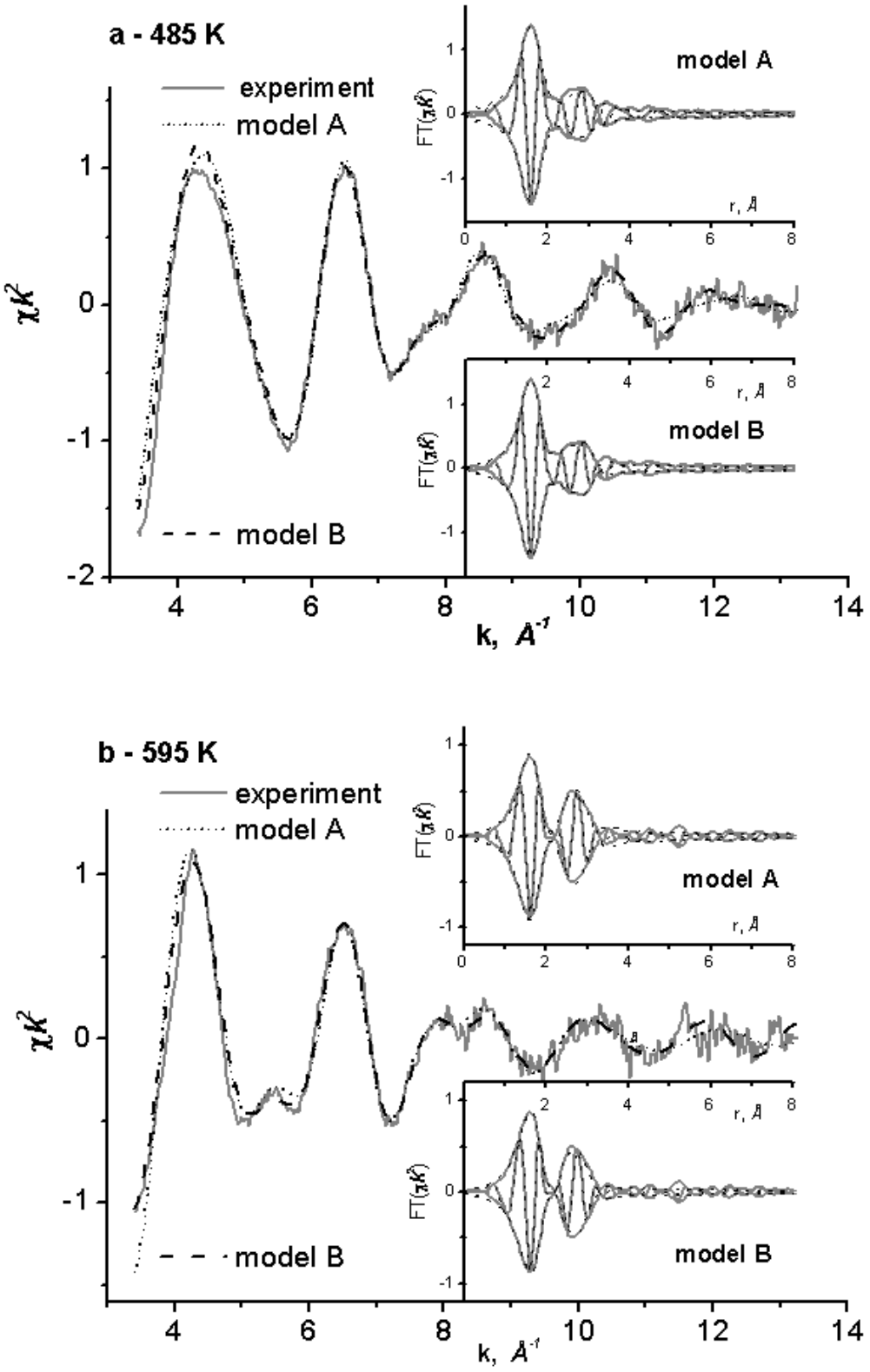
a - 485 K
experiment
model A
model B
model A
model B
FT(χk²)
r, Å
χk²
k, Å⁻¹
b - 595 K
experiment
model A
model B
model A
model B
FT(χk²)
r, Å
χk²
k, Å⁻¹

Figure 9